Proceedings of the 21st ICSMGE, Vienna, Austria, 14 – 19 June 2026. Pistrol, Adam & Schweiger (eds.)
Published by: ÖGG, Austrian Society for Geomechanics, Salzburg, Austria, ISBN 978-3-9503898-4-5
https://doi.org/10.53243/ICSMGE2026-501

Numerical analyses and innovative design approaches for piled foundations

Francesco Potini
Università degli Studi Niccolò Cusano, Roma, Italia, francesco.potini@unicusano.it

Giulia M. B. Viggiani
University of Cambridge, Cambridge, UK, gv278@cam.ac.uk

Riccardo Conti
Università degli Studi di Roma "Tor Vergata", Roma, Italia, riccardo.conti@uniroma2.it

ABSTRACT: The ultimate behaviour of piled foundations under generalised loads was recently investigated from an experimental, numerical and theoretical point of view, with the aim of developing innovative design solutions to overcome the conservatism of conventional approaches. Simple limit analysis solutions have been proposed recently to compute the failure domain of pile groups under vertical eccentric loads, while reliable and consistent solutions for the case of inclined loads are still lacking. This paper presents the main results of a numerical study aimed at investigating the failure behaviour of pile groups embedded in a clayey soil deposit under combined loading. Advanced three-dimensional analyses were performed with the Finite Element code Abaqus. To reproduce the nonlinear behaviour of reinforced concrete piles, a damage plasticity model was used for the concrete, while reinforcement bars were modelled as equivalent elastoplastic shell elements. The soil was modelled as a standard elastic-perfectly plastic material with a Tresca failure criterion to represent the undrained soil behaviour in a total stress analysis. Numerical results permitted to identify the main physical mechanisms occurring within the soil-foundation system, as well as the dimensionless groups governing the problem. Based on these results, an innovative theoretical method was developed to compute the ultimate domain of a pile group subject to inclined-eccentric loads. The method accounts for the combined effect of group geometry, structural and geotechnical capacity of the single piles, and loading direction on the actual plastic mechanism occurring within the group and the corresponding failure envelope.

KEYWORDS: bearing capacity; finite-element modelling; limit state design/analysis; piles & piling.

1 INTRODUCTION

The ultimate response of pile groups has been addressed by many authors, with the aim of defining more rational procedures for their design under generalised vertical (*V*), horizontal (*H*) and moment (*M*) loads (Di Laora *et al*., 2019; Iovino *et al*., 2021; Di Laora *et al*., 2022; Gorini & Callisto, 2022; Potini *et al*., 2023). Three-dimensional (3D) failure envelopes have been computed applying the lower bound (LB) and upper bound (UB) theorems of limit analysis, neglecting the contribution of the raft to the overall resistance, and assuming a classical fixed-head/long pile failure mechanism under horizontal loads (Broms, 1964a, 1964b).

Experimental and numerical works (Gerolymos & Papakyriakopoulos, 2016; Psychari & Anastasopoulos, 2022; Sakellariadis & Anastasopoulos, 2024a; Sakellariadis & Anastasopoulos, 2024b) have shown that the horizontal capacity of pile groups is related to the actual failure mode of the single piles, which in turn depends on the *M–V* loading applied to the foundation. As the connecting raft can rotate under horizontal forces, the restraint condition at the pile's head does not necessarily imply that the pile head does not rotate. As a result, failure of pile groups occurs with strong *M–H* and *V–H* coupling that cannot be reproduced by the solutions in the available literature, which assume a priori a fixed-head failure mechanism.

Recently, Sakellariadis & Anastasopoulos (2024b) and Di Laora *et al*. (2025) developed novel approaches, based on the limit equilibrium method, to assess the ultimate response of pile groups under combined loading conditions. The former focused on the behaviour of pile groups in sand, where the piles do not exhibit a clear punching mechanism under axial loads, and the group does not show any loss of horizontal capacity due to *V–H* coupling. The latter developed a simplified method able to take into account both the *M-H* and the *V-H* coupling.

This work focuses on the undrained ultimate response of pile groups in clay. The results of advanced 3D FE analyses are used to highlight the main factors governing the behaviour of these systems under combined loading conditions. Moreover, starting from the response of the single pile under generalised loads, a new LB solution is proposed to compute the 3D failure domain of the pile group (Potini *et al*., 2025).

2 NUMERICAL MODEL

2.1 *Problem definition*

Figure 1(a) shows the foundation system under investigation, consisting of a group of piles connected by a raft, assumed to be clear of the soil, and subjected to generalised loads.

The pile group is embedded in a homogeneous overconsolidated clay layer, with unit weight, $\gamma = 20$ kN/m^3, undrained shear strength, $s_u = 100$ kPa, and Young's modulus in undrained conditions, $E_u = 20$ MPa. Different group layouts were analysed, by varying the pile spacing (s) and the number of piles along the x (n_{px}) and y (n_{py}) directions, while keeping constant the length of the piles, L (= 15 m) and their diameter, d (= 1 m). The structural section of the piles comprises 27ϕ26 longitudinal rebars with a cover of 50 mm. Figure 1(b) shows the *V–M* interaction domain of the pile section (Potini & Conti, 2024), together with the values of the undrained bearing capacity of the piles in compression, N_u, and in tension, S_u obtained from numerical analyses (Potini *et al*., 2025).

The behaviour of a row of three piles (3×1), with spacing $s/d = 3$, was analysed first to identify the failure modes of pile groups under *V–H–M* loading. Then, to understand how the pile configuration affects the ultimate response of the group, an extensive numerical parametric study was conducted on a single row of piles, varying their number ($n_p = 2 \div 6$) and spacing ($s/d = 3 \div 6$).

Only positive M/H ratios were applied in this study, which is typically the most relevant condition for the ultimate limit state design of foundations in seismic areas, where H and M derive from the inertia forces acting on the structure. Moreover, only pile spacings $s/d \geq 3$ were considered, to minimise pile-to-pile interaction effects under both vertical and horizontal loads.

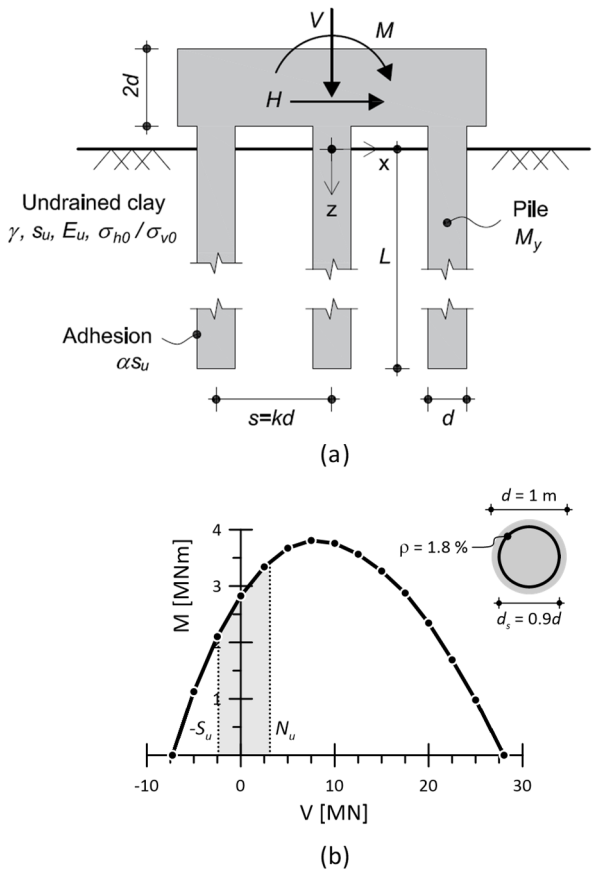

Figure 1. Problem definition: (a) 3×1 pile group; (b) *V*–*M* interaction domain of the RC pile section

2.2 *FE model*

Three-dimensional total stress analyses were carried out with the FE code Abaqus (ABAQUS, Inc., 2017), assuming undrained conditions. Eight-node linear brick elements with reduced integration were used to model the soil and the concrete, while the reinforcement bars within the reinforced concrete (RC) piles were modelled as an equivalent steel pipe embedded in and perfectly bonded to the concrete continuum elements, by using four-node linear shell elements with reduced integration. The steel pipe has the same area of the longitudinal rebars (ρ = 1.8%), and an equivalent diameter $d_s = 0{\cdot}9\,d$.

2.3 *Constitutive models*

The undrained behaviour of the clay was modelled as linear elastic–perfectly plastic with Tresca failure criterion and associated flow rule (Young's modulus, $E = E_u$; Poisson's ratio, ν = 0.495; cohesion, $c = s_u$).

An isotropic elastic–perfectly plastic constitutive model was used for the reinforcement steel pipe (B450C steel class), with a von Mises failure criterion and an associated flow rule.

The raft was modelled as a weightless linear elastic material while the mechanical behaviour of the concrete piles was reproduced using the concrete damaged plasticity (CDP). The complete set of evolution equations, as well as a thorough discussion on the effectiveness of the CDP model in reproducing the structural behaviour of RC piles, were reported by Potini & Conti (2024).

The pile–soil interface was modelled with tensionless contact elements, which allow both sliding and separation. An elastoplastic frictional behaviour was assumed for the interface, with a threshold value $\tau_{max} = \alpha s_u$ for the maximum allowable shear strength, where $\alpha = 0.5$ is the interface adhesion factor.

3 NUMERICAL RESULTS

3.1 *Pile group under vertical eccentric loads*

The overall response of the 3×1 pile group under vertical eccentric loads is summarised in Figure 2, showing the ultimate (*V*, *M*) domain of the pile group, together with the *M*–θ curves at specific failure points (A to D), indicating the progressive mobilisation of the moment capacity with increasing the rotation of the connecting raft. For each applied vertical load, the two contributions stemming from the axial load on the piles (M_{ax}) and from the formation of plastic hinges at the piles head (M_b) are isolated, thus highlighting the relative importance of the two concurrent resistance mechanisms on the total moment capacity of the group (M_u).

As can be seen both theoretically and numerically, M_b exhibits minor variations with increasing *V*. In contrast, M_{ax} decreases substantially with the applied vertical load, up to the limit condition where $V_u = n_p N_u$ and $M_{ax} = 0$. As a result, most of the moment capacity of the pile group under relatively large vertical loads relies on the plastic moment capacity of the piles' cross-section.

As a final comment, M_{ax} requires cap rotations of approximately 0.01÷0.015 rad to be fully mobilised, while M_b is attained at relatively higher rotations (θ ≈ 0.03 rad). The rotations at which the two contributions are mobilised derive from different physical factors. The former (M_{ax}) is related to the vertical displacement at which the axial capacity of the outermost pile is attained, while the latter (M_b) depends on the soil–pile relative stiffness and on the pile moment capacity. As a result, the values obtained for this reference layout cannot be generalised to other pile group layouts and soil deposits.

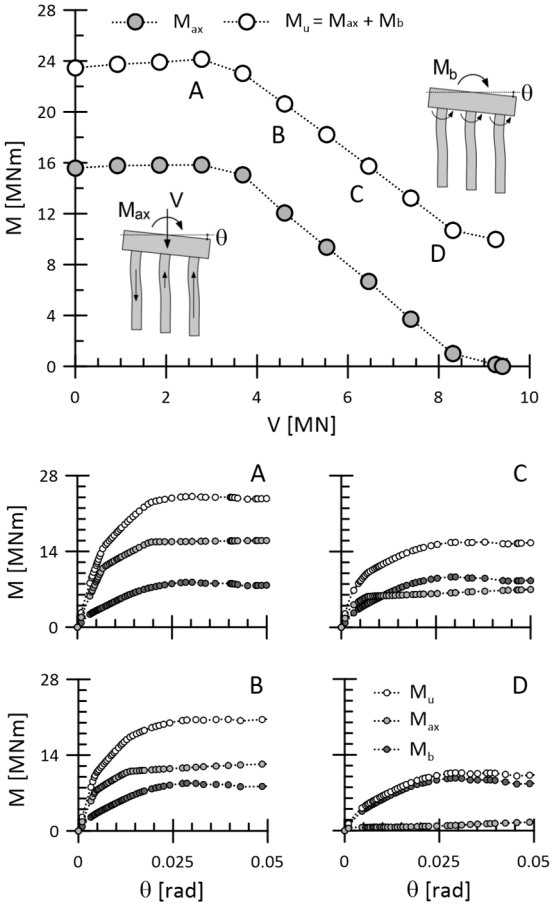

Figure 2. Failure domain of a 3×1 pile group under *V*-*M* loading

3.2 *Pile group under generalised loads*

Figure 3 shows some sections of the ultimate domain of the 3×1 group in the plane (H, M) for three fixed V/V_u ratios (= 0, 0.6, 0.8), and in the plane (V, H) for three fixed values of M (= 0, 12, 20 MNm). The numerical results indicate that there is a significant coupling between the horizontal capacity of the pile group, H_u, and the V-M loads acting on the foundation. Specifically, H_u decreases rapidly as M increases (at constant V), Figure 3(a), while an increase in vertical load (at constant M) induces an initial increase in H_u, due to the increase in M_{yb} within the piles, followed by a significant reduction in horizontal capacity, Figure 3(b).

An explanation of the ultimate response exhibited by the 3×1 pile group is provided by the contours of the axial strain mobilised within each pile referring to specific points of the domain. As illustrated for the section characterised by $V/V_u = 0$ in Figure 3(a), the rotation of the raft increases with the applied moment, resulting in a different kinematic constraint imposed on the pile head and a different moment transmitted from the raft to the piles. As a result, the piles exhibit different failure mechanisms, starting with the formation of two plastic hinges, of opposite sign (points A and B); passing through the activation of a single plastic hinge at depth (points C, D, E and F); up to the development of a single plastic hinge at the head of the piles, which corresponds to $H = 0$ (point G). In all cases, the three piles within the group exhibit very similar behaviour, with a slight difference in the position of the plastic hinge in depth, due to the different axial load acting on each pile. Since an increase in the moment acting at the head of the pile causes a reduction in the horizontal limit load, the horizontal resistance of the entire foundation reduces as M increases. The same response is observed from the axial strain contours in Figure 3(b), referring to the curve at $M = 0$: for small values of the vertical load (points A and B), the pile group reaches the failure condition with a marginal rotation of the raft, hence the piles reach failure under horizontal action with the formation of two plastic hinges. As V increases (in this case, approximately $V \geq 4$ MN), the connection raft begins to rotate and the piles develop a single plastic hinge at failure, with a significant reduction in H_u (points D and E).

4 THEORETICAL MODEL

This section presents a new theoretical framework to compute the 3D failure domain of pile groups in clay. To this end, an iterative LB procedure is implemented, providing a statically admissible distribution of axial and shear forces within the piles, for groups of any shape subjected to any V–H–M load.

The main ingredients of the model are: (a) the M–V interaction diagram of the pile cross-section, defining the pile structural behaviour; (b) the axial limit loads of the single pile in compression (N_u) and uplift ($-S_u$); (c) the M–H failure domain of the single pile proposed by Potini and Conti (2024). The authors apply the limit equilibrium method to derive a closed-form expression of $H_u(M)$, after defining (i) a horizontal resistance profile per unit length along the pile and (ii) the acting moment as a fraction of the yielding moment of the pile section, i.e. $M = \beta_y \cdot M_{yb}$, where $-1 \leq \beta_y \leq 1$. The two conditions $\beta_y = -1$ and $\beta_y = 0$ correspond to the failure mechanism of a fixed- and free-head pile, respectively. As β_y increases, the plastic hinge at depth tends to develop closer to the pile head, causing a progressive reduction of H_u. In the limit condition $\beta_y = 1$, when $M = M_{yb}$ at the pile head, the two plastic hinges collapse into one and $H_u = 0$.

The main assumptions of the model are: (a) the piles exhibit a rigid–perfectly plastic behaviour, under both axial and horizontal loads; (b) the connection between the piles and the raft consists in a rigid plastic internal fixity; (c) the raft is a rigid body not in contact with the soil; (d) all piles within the group share the same failure mode under horizontal loads, which implies a unique value of $\beta_y = M_i/M_{ybi}$; (e) the axial force is approximately constant along the uppermost portion of the piles involved in the failure mechanism (up to $5 \div 8$ d for typical RC piles). In addition to this, any possible geotechnical coupling between axial and lateral failure mechanisms of the single pile is disregarded (Sakellariadis & Anastasopoulos, 2024b), as well as pile-to-pile interaction effects under vertical and horizontal loads (Potini *et al*., 2023).

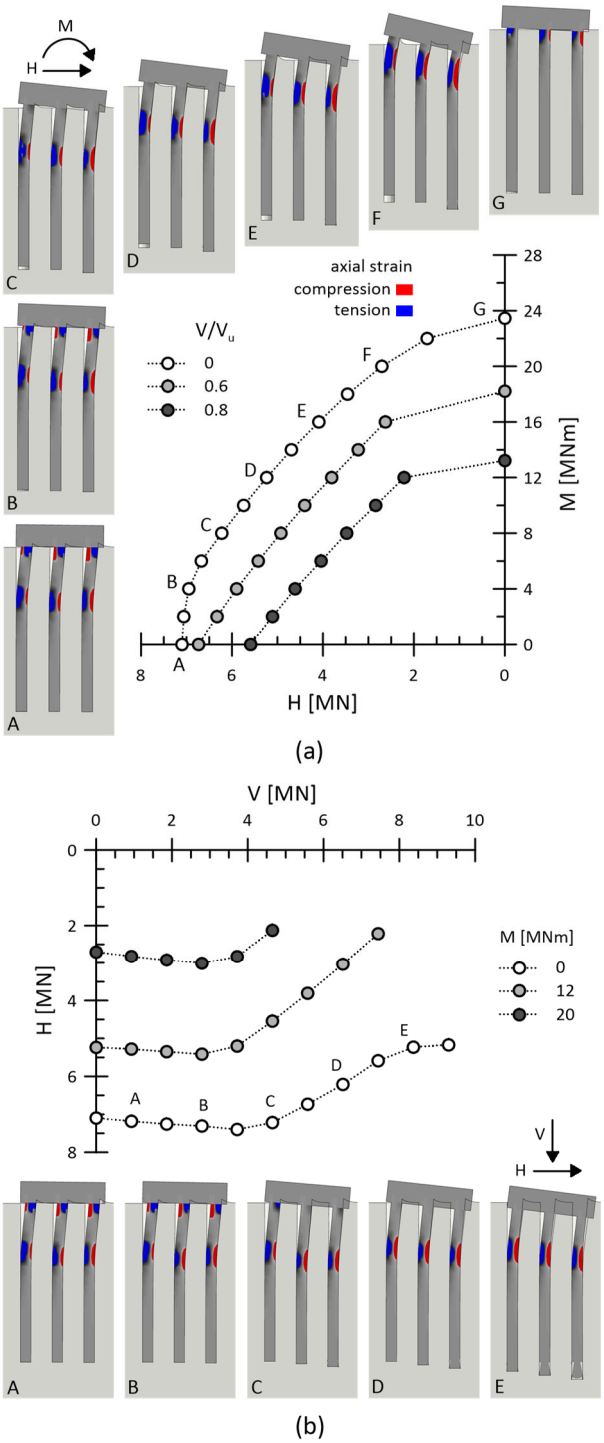

Figure 3. Sections of the numerical failure envelope of a 3×1 pile group in the planes: (a) H:M; and (b) H:V, together with the contours of axial strains within the piles at some reference failure points.

4.1 *Coupling between V–M loads and horizontal capacity*

The construction of the 3D failure domain starts from its section in the *V*:*M* plane, at $H = 0$ (Iovino *et al*., 2021; Di Laora *et al*., 2022; Potini *et al*., 2023). The latter is computed extending the LB procedure implemented by Potini *et al*. (2023), to account for both M_{ax} and M_b. To this end, the equilibrium equations of the pile group are solved including the contributions M_{ybi}, stemming from the plastic hinge at the head of each pile.

The key idea for assessing the observed coupling between the lateral capacity of the pile group and the applied vertical and moment loads is simply making the coefficient β_y in the closed-form expressions of H_{ui} (Potini & Conti, 2024) a function of *V* and *M*. In this way, the horizontal limit load of each pile is related to the expected failure mode of the group.

A schematic representation of the adopted function $\beta_y(V, M)$ is given in Figure 4. As indicated by FE results of the 3×1 group: a deep failure mechanism is expected for points along the boundary of the *V*–*M* domain ($\beta_y = 1$); a shallow mechanism occurs for small (*V*, *M*) values, defining an internal region (kernel) characterised by the classical double-hinge formation ($\beta_y = -1$); for $(V, M) = (V_u, 0)$, horizontal failure of the piles is attained with only a marginal mobilisation of the bending capacity at the head ($\beta_y = 0$). A linear variation of β_y is assumed between these reference points. Moreover, to describe the different coupling observed between *V*–*H* and *M*–*H* loading components (see e.g. Figure 3), the internal kernel is obtained by a non-homothetic scaling of the *V*–*M* failure domain (at $H = 0$), that is $(V, M) = (S_{\beta V} \cdot V_u,\ S_{\beta M} \cdot M_u)$, where $S_{\beta V} \le 1$ and $S_{\beta M} \le 1$ are suitable scaling factors.

These coefficients must be physically related to the dimensionless factors mainly affecting the pile cap rotation at failure, that is: $\Pi_1 = (n_p - 1) \cdot k$, with $k = s/d$, related to the rocking inertia of the pile group, and $\Pi_2 = d \cdot N_u / M_{yb0}$, with $M_{yb0} = M_{ybi}(V_i = 0)$, expressing the ratio between the axial and moment capacity of the single pile. To obtain suitable expressions for $S_{\beta V}$ and $S_{\beta M}$, an extensive FE parametric study was carried out, exploring the effect of Π_1 and Π_2. The FE results are summarised in Figure 5, where numerical values of $S_{\beta V}$ and $S_{\beta M}$ are reported as a function of $\Pi = \Pi_1 \cdot \Pi_2$, together with their hyperbolic best fit, given by:

$$S_{\beta M}(\Pi) = \frac{0.70 \cdot \Pi^{2.4}}{340 + \Pi^{2.4}} \tag{1}$$

$$S_{\beta V}(\Pi) = \frac{0.88 \cdot \Pi^{1.7}}{25 + \Pi^{1.7}} \tag{2}$$

As expected, both $S_{\beta V}$ and $S_{\beta M}$ increase with Π, indicating that the internal kernel enlarges with increasing the inertia of the group (Π_1) and the ratio of axial/moment capacity of the piles (Π_2), because of the smaller cap rotation induced by the horizontal load at failure.

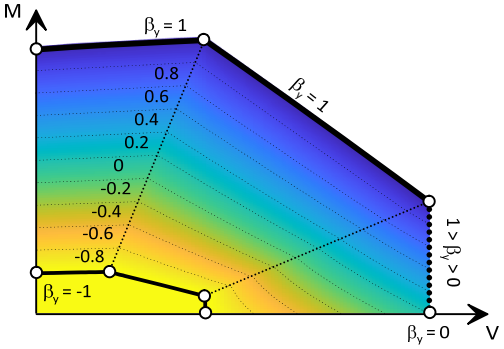

Figure 4. Theoretical model: schematic representation of the assumed linear variation of $\beta_y(V, M)$

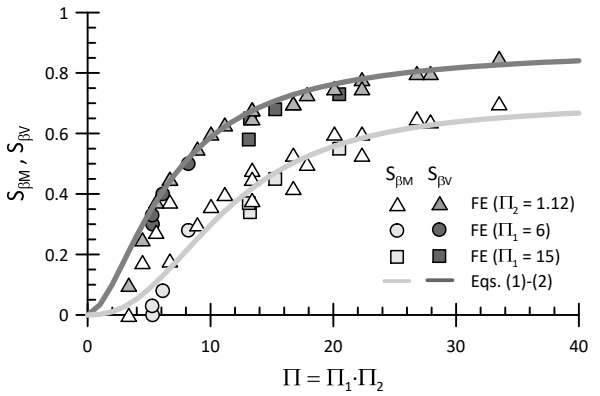

Figure 5. Theoretical model: numerical values and theoretical best fit of the scaling factors $S_{\beta M}$ and $S_{\beta V}$

4.2 *Equilibrium equations*

As shown schematically in Figure 6, for each point within the *V*–*M* failure envelope (at $H = 0$), a LB distribution of the axial loads within the piles is obtained by solving the two equilibrium equations of the pile group (Equations (3) and (4)). Then, the corresponding horizontal limit load, H_u, is computed by summing up the lateral capacity of each pile (Equation (5)):

$$V = \sum_{i=1}^{n_p} V_i \tag{3}$$

$$M = \sum_{i=1}^{n_p} V_i x_i + \beta_y \sum_{i=1}^{n_p} M_{ybi} \tag{4}$$

$$H_u = \sum_{i=1}^{n_p} H_{ui} \tag{5}$$

where $\beta_y = \beta_y(V, M)$. As $M_{ybi} = M_{yb}(V_i)$, the system of two Equations (3)-(4) must be solved iteratively; at each iteration, an incremental procedure can be implemented to find a compatible distribution of axial forces within the piles (Potini *et al*., 2023). Furthermore, by using the closed-form expressions of H_{ui} proposed by Potini and Conti (2024) to compute the horizontal capacity of the single pile, it turns out that $H_{ui} = H_{ui}(V, M)$ through $\beta_y(V, M)$ and $M_{yb}(V_i)$.

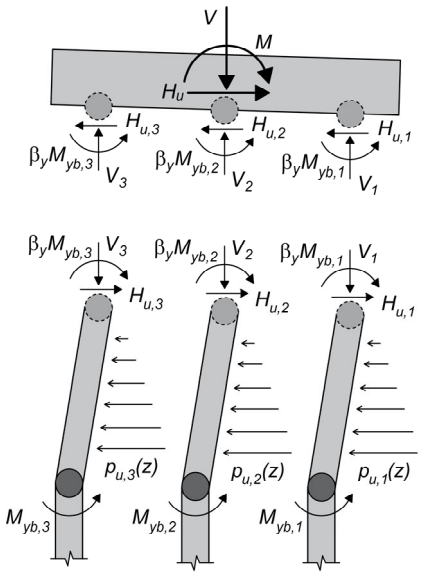

Figure 6. Theoretical model: layout of external loads and internal forces acting on the pile group

4.3 *Comparison between FE and theoretical results*

Figure 7 shows a comparison between the 3D numerical failure domain of the 3×1 pile group and the one predicted by the proposed method. In the *V*:*M* plane (Figure 7(a)), the LB envelope coincides with the solution by Di Laora *et al*. (2019). The theoretical model reproduces well the numerical *M*–*H* and *V*–*H* coupling, indicating that the assumption of linear variation of β_y does not oversimplify the actual mechanisms occurring within the foundation–soil system. Small differences between numerical and theoretical results are mainly due to pile-to-pile interaction effects induced by generalised loads, not included in the analytical framework.

4.4 *Some remarks on the proposed theoretical model*

Based on the proposed theoretical model, the transition between deep and shallow failure mechanisms is governed by the two dimensionless factors $\Pi_1 = (n_p\text{-}1)\cdot k$ and $\Pi_2 = d\cdot N_u/M_{yb0}$, setting the size of the internal kernel through the scaling factors $S_{\beta V}$ and $S_{\beta M}$. As a result, an implicit assumption underlying the proposed model is that pile groups with different geometry, but same Π_1 and Π_2, will share the same ultimate behaviour when subjected to the same dimensionless generalised loads, i.e.: V/V_u, H/H_u and M/M_u, with $V_u = n_pN_u$, $H_u = n_pH_{u0}$ and $M_u = M_u|_{V=0}$. Worth noting, for a row of n_p identical and equally spaced piles, the moment load can be conveniently normalised by the quantity $M_u = [n^*s\cdot(N_u+S_u)/2+n_pM_{yb0}]$, with $n^* = n_p^2/4$ and $n^* = (n_p^2\text{-}1)/4$ for even and odd n_p values, respectively, expressing the maximum failure moment of the pile group.

To validate such assumption, Figure 8 shows the numerical and theoretical failure domains of a 4×1 ($s/d = 5$) and a 6×1 ($s/d = 3$) pile group, both characterised by $\Pi_1 = 15$ and $\Pi_2 = 1.12$. Specifically, in Figure 8 are shown three sections of the failure envelopes in the (a) *V*:*M* ($H = 0$), (b) *H*:*M* ($V/V_u = 0.1$) and (c) *H*:*V* ($M = 0$) normalised planes. As apparent, the numerical failure domains of the two pile groups have the same shape both in the *H*:*M* and in the *V*:*H* dimensionless planes, indicating that the internal core does have the same extension for the two pile configurations. Minor differences in FE results are essentially due to pile-to-pile interaction effects, slightly affecting the ultimate behaviour of the 6×1 pile group ($s/d = 3$), while absent in the 4×1 group ($s/d = 5$). Such effects are not included in the theoretical model, whose predicted failure envelopes for the two pile groups are perfectly overlaid.

The validity of the theoretical assumption is confirmed by inspection of the contours of axial deformations at failure within the piles in Figure 8b, referred to the same 4×1 and 6×1 pile groups subjected to the same reference load paths ($V/V_u = 0.1$, $M/M_u = 0, 0.9$). The two pile groups exhibit the same failure mechanisms, characterised by the formation of two plastic hinges at $M = 0$, and a single plastic hinge at $M = 0.9M_u$.

5 CONCLUSIONS

This study investigated the ultimate behaviour of pile groups embedded in cohesive soils under combined vertical, lateral, and moment loading. 3D finite element analyses were used to identify the key plastic mechanisms and the main factors influencing the response at failure of these systems.

The main findings can be summarized as follows:

- Under significant vertical loads, the moment capacity of the pile group is largely governed by the plastic bending resistance of the individual pile sections, particularly relevant for large-diameter RC piles in seismic regions.
- Three distinct failure mechanisms (shallow, intermediate, deep) were observed, each associated with different mobilisation of axial and bending capacity. The governing failure mechanism is primarily controlled by the raft's ultimate rotation, which depends on the applied vertical and moment loads. This leads to strong coupling between *M*–*H* and *V*–*H* at failure.
- For a given *V*–*M* load combination, the failure conditions of the pile group can be described through two dimensionless parameters: $\Pi_1 = (n_p\text{–}1)\cdot k$ and $\Pi_2 = d\cdot N_u/M_{yb0}$, which represent the group's rocking inertia and the ratio between axial and moment capacity of a single pile, respectively.

Based on the theoretical model for single piles under combined loads by Potini & Conti (2024), the proposed LB framework captures all the possible failure modes of the pile group observed from numerical analyses. The model effectively reproduces the strong *M*–*H* and *V*–*H* interaction and ensures full equilibrium between internal and external forces.

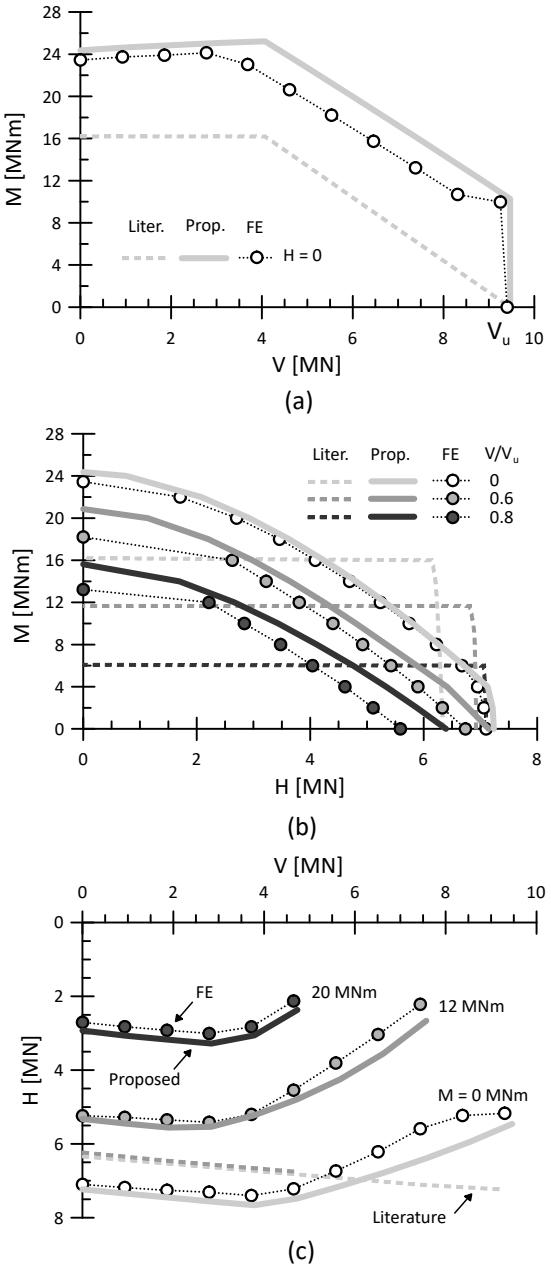

Figure 7. Three-dimensional failure domain of a 3×1 pile group under generalised loads. Sections in the three planes: (a) V:M, (b) H:M and (c) V:H. Comparison between FE results, literature methods and predictions of the proposed theoretical model.

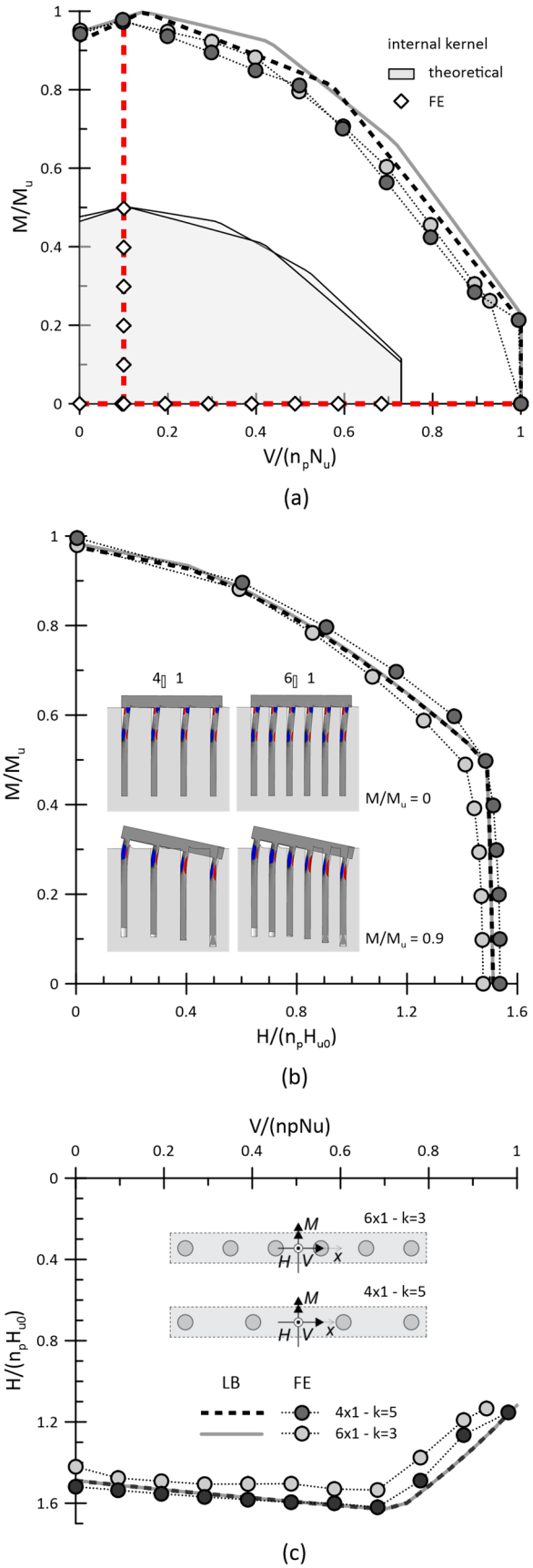

Figure 8. Numerical and theoretical failure domains of 4×1 (s/d = 5) and 6×1 (s/d = 3) pile groups. Sections in the normalised planes: (a) V:M (H = 0), (b) H:M (V/V_u = 0.1) and (c) H:V (M = 0).

6 ACKNOWLEDGEMENTS

Financial support for this research was provided by Regione Lazio (Italy) and Italferr S.p.A. within the programme POR-FSE 2014-2020 (Grant Agreement no. F83C22000770005). The Authors wish to acknowledge dr. Letizia Berardi, dr. Andrea F. Rotunno for many fruitful discussions during the initial stages of the work.

7 REFERENCES

ABAQUS, Inc. (2017). ABAQUS 2017 user's manual. Dassault Systèmes Simulia Corp.

Broms, B. B. (1964a). Lateral resistance of piles in cohesive soils. J. Soil Mech. Found. Div. 90, No. 2, 27–63.

Broms, B. B. (1964b). Lateral resistance of piles in cohesionless soils. J. Soil Mech. Found. Div. 90, No. 3, 123–156.

Di Laora, R., de Sanctis, L. & Aversa, S. (2019). Bearing capacity of pile groups under vertical eccentric load. Acta Geotech. 14, No. 1, 193–205.

Di Laora, R., Iodice, C. & Mandolini, A. (2022). A closed-form solution for the failure interaction diagrams of pile groups subjected to inclined eccentric load. Acta Geotech. 17, No. 8, 3633–3646.

Di Laora, R., Cesaro, R., Iodice, C., Iovino, M., de Sanctis, L. (2025). A closed form solution for the generalised failure envelope of a pile group, Soil Dyn. Earthq. Engng 199, 109623.

Gorini, D. N. & Callisto, L. (2022). Generalised ultimate loads for pile groups. Acta Geotech. 17, No. 6, 2495–2516.

Gerolymos, N. & Papakyriakopoulos, O. (2016). Macroelement modelling of laterally loaded piles and pile-groups. 1st ICONHIC 2016, Chania, Greece.

Iovino, M., Maiorano, R. M. S., De Sanctis, L. & Aversa, S. (2021). Failure envelopes of pile groups under inclined and eccentric load. Géotechnique Lett. 11, No. 4, 247–253.

Potini, F. & Conti, R. (2024). Horizontal bearing capacity of RC piles in cohesive soil: numerical and theoretical modelling. Comput. Geotech. 175, 106638.

Potini, F., Gorini, D. N. & Conti, R. (2023). Rigorous lower and upper bounds for the generalised failure loads of pile groups. Géotechnique Lett. 13, No. 2, 1–7.

Potini, F., Viggiani, G.M.B., Conti, R. (2025). Interaction domains of pile groups in cohesive soils under generalised loads. Géotechnique, 10.1680/jgeot.24.01210.

Psychari, A. & Anastasopoulos, I. (2022). Combined loading of RC pile groups in clay accounting for N–M interaction. Soil. Dyn. Earthq. Eng 163, No. 107, 490.

Sakellariadis, L. & Anastasopoulos, I. (2024a). On the mechanisms governing the response of pile groups under combined VHM loading. Géotechnique 74, No. 9, 840–861, https://doi.org/10.1680/jgeot.21.00236.

Sakellariadis, L. & Anastasopoulos, I. (2024b). Analytical 3D failure envelopes for RC pile groups under combined loading: a generalised design approach. Soil Dyn. Earthq. Engng 181, 108570.